Photoacoustics 12 (2018) 55–66

Contents lists available at ScienceDirect

Photoacoustics

journal homepage: www.elsevier.com/locate/pacs

Research article

Absorption spectra of nanodiamond aqueous dispersions by optical absorption and optoacoustic spectroscopies

L.O. Usoltseva[a], D.S. Volkov[a], D.A. Nedosekin[b], M.V. Korobov[a], M.A. Proskurnin[a], V.P. Zharov[b]

[a] Chemistry Department, Lomonosov Moscow State University, Moscow, 119991, Russia
[b] Philips Classic Laser Laboratories, University of Arkansas for Medical Sciences, Little Rock, Arkansas, 72205, USA

ARTICLE INFO

Keywords:
Optoacoustic spectroscopy
Multispectral optoacoustic spectroscopy
Optically dense samples
Nanodiamonds
Nanodiamond aqueous dispersions
Nanodiamond fractionation

ABSTRACT

The multispectral modality and technique for optically dense samples of optoacoustic spectroscopy were applied to measure spectra and high absorbances of concentrated aqueous dispersions of undoped nanodiamonds. The data from optoacoustic and optical transmission measurements and DSC data of the mean particle size by the Gibbs–Kelvin equation are compared to estimate the difference in composition of various nanodiamond trademarks. Optoacoustic spectra confirm the contribution of surface dimer chains into the absorption of nanodiamonds in the long wavelength range. Optoacoustic and conventional absorption spectra of aqueous solutions of nanodiamond fractions after centrifugation (15300*g*) and ultracentrifugation (130000*g*) revealed a separation of a highly absorbing non-diamond sp^2 phase. The two-step separation by ultracentrifugation followed by extra centrifugation made it possible to isolate a highly absorbing and soluble nanodiamond phase with the particle size of 3.6 nm, showing a change in spectra compared to the starting nanodiamond material.

1. Introduction

Unique properties of detonation nanodiamond (**ND**) materials find various applications in the state-of-the-art branches of science and technology [1–6]. They are used in the formation of composites, electronic instruments, catalysts [1,2], and as new sorbents [3,5–7]. These materials are also promising for biomedical applications [8,9]. Here, ND can be used as fluorescent and contrast agents in clinical diagnostics and diagnostic sensors [10–12], platforms for drug delivery [13,14], enterosorbents, in cellular surgery, anticancer therapy, and many other areas [15]. The interest to ND materials have resulted in the growth of their production and the development of the production technology, which made NDs commercially available. Many applications of ND utilize their ability to readily form concentrated aqueous dispersions [16].

Before application, especially in the form of aqueous solutions, NDs need to be thoroughly characterized. The control of the surface chemistry and particle size are in demand, as may properties of ND materials depend on the surface properties and NDs tend to agglomerate to form larger particles [17,18]. Hereby, the methods and techniques for non-destructive characterization and assessment of NDs are required. The characterization of NDs have become even more topical recently with the development of new techniques of ND surface modification and functionalization [19], and ND applications as building blocks in producing films and in the composite synthesis of microdiamonds [20]. Many of these applications as well as more traditional applications of nanodiamonds as lubricants and as novel nanofluids [21] require concentrated aqueous dispersions or hydrosols.

Optical absorption spectroscopy is a valuable tool for assessing and characterizing nanodiamonds, their aqueous solutions, and films [22]. Optical properties of ND aqueous dispersions depend not only on the ND concentration, but also on the production technology, size of particles, and the presence of impurities. Light absorption of NDs in the optical region is associated with the presence of sp^2 carbon, especially if disintegrated by the stirred-media milling process [23–25] and dimer (Pandey) chains being formed during surface reconstruction [26,27]. Also, this can be associated with impurities, which include nitrogen, silicon, oxygen, hydrogen, and various metals [28,29]. Also, optical absorption spectroscopy in combination of fluorescence modalities is used for characterization of doped or nitrogen–vacancy (NV) nanodiamonds used as tags in many biological applications [30–32].

Conventional optical absorption spectroscopy (spectrophotometry) and photothermal (thermal-lens) spectroscopy have been used previously for quantification and analysis of spectra of ND aqueous dispersions [22,25,26]. The generic consideration of optical properties of meteoritic nanodiamonds was made as well [33]. However, the use of spectrophotometry is limited by strong beam attenuation due to high absorptivities and scattering in highly concentrated ND solutions. Also, the response of a transmission spectrophotometer is both due to absorption and scattering, i.e., it is a total extinction measurement. Thus, there also exists the problem of separation of ND extinction spectra into absorption and scattering components [25], which is not fully resolved yet, which hinders the understanding of many relevant ND properties.

Additionally, the interest recently has been focused on ND

https://doi.org/10.1016/j.pacs.2018.10.003
Received 15 June 2018; Received in revised form 7 October 2018; Accepted 23 October 2018
Available online 28 October 2018

fractionation as it may produce the materials with the minimum particle size [25,26,29,34–42] and gives particles with defined aggregate sizes for various applications like film and gel production [15]. Previously, it was reported that ND fractions have different surface chemical composition [40]; FTIR and especially DLS [35,36,43] are commonly used methods for fraction characterization, but the absorption spectra were not considered in full.

We propose optoacoustic (**OA**) spectroscopy along with UV/vis and differential scanning calorimetry (**DSC**) measurements for qualifying ND samples. The advantage of the approach is that OA modalities respond to absorption (at least for dilute samples) and that light-scattering media are acoustically transparent to a certain extent [44,45]. Thus, this method can be used for measurement of high absorbances characteristic for practically relevant ND samples. Therefore, the comparison of OA and optical absorption data can be used for the rapid estimation of the ratio of absorption and scattering. Thus, we compare UV/vis and OA spectra of different ND aqueous dispersions and their fractions made by centrifugation and ultracentrifugation.

2. Materials and methods

2.1. Instruments

2.1.1. OPO-based multiwavelength microscopic optoacoustic setup

The multispectral OA-setup was built using an Olympus IX81 inverted microscope platform (Olympus America, Center Valley, PA), and a tunable pulsed optical parametric oscillator (Opolette HR 355 LD, OPOTEK, Inc., Carlsbad, CA) with the spectral range, 400–2200 nm; pulse width, 5 ns; pulse repetition rate, 100 Hz; and energy fluence range, 0.1–10^4 mJ/cm^2 [46]. For OA measurements, all objectives were 10× (Olympus America). The laser-induced ultrasound waves were detected in a transmission configuration using an ultrasound transducer (V-324-SE, 25 MHz; focal length 12 mm, Panametrics) immersed into the ultrasonic gel above the sample.

ND solutions were measured by placing a solution aliquot (8.6 μL) in a specially designed cuvette, which is a Secure-Seal polymer film (Invitrogen Corp., Carlsbad), which forms a sample well (optical path length 120 μm) between two thin microscope slides.

The optoacoustic spectra were measured for the whole working range of the OPO (410–710 nm, with a step of 1 nm). The excitation energy spectrum were obtained using an energy meter (PE10-SH, OPHIR) for the selected experimental conditions. Then, the obtained optoacoustic spectra were corrected to the same energy of the excitation using the excitation energy spectrum [47]. The short- and long-wave parts of the spectra (410–430 and 690–710 nm) were usually discarded due to low signal-to-noise ratios resulted from a low energy of the excitation. The rest of the spectra were subjected to a standard 2nd order Savitzky–Golay digital filter procedure (using OriginPro 2015 for Windows).

2.1.2. Optoacoustic setup for optically dense solutions

The schematic of the optoacoustic setup for optically dense solutions is presented in Fig. S1 (Supplementary information). The details including signal processing and absorbance calculations are given previously [44]. For the generation of OA-signals in the medium under study, the radiation of the second harmonic (532 nm) of a pulsed Nd:YAG laser (LS-2137-3, LOTIS TII) was used. The laser pulse duration (FWHM) is 22 ns, which was measured with a photodiode. The laser pulse repetition rate was 50 Hz, which allowed the detection of the OA-signal in 3 s (at 128 signal averages) and thereby neglecting any short-time fluctuations. The laser pulse energy was attenuated with neutral filters (990-0704, Eksma Optics) and did not exceed 1 mJ; corresponding laser fluences did not exceed few mJ cm^{-2}. After the attenuator, a convex lens is used to homogenize the light distribution in the beam cross-section and expand the beam diameter to 12 mm at the surface of the sample. The laser radiation was directed to the OA-cell with a quartz prism.

The OA-cell for this setup consisted of a polished quartz plate (6 mm, thickness and 25 mm, diameter) and a quartz cylinder (5 mm, thickness; 25 mm, the outer diameter; 20 mm, the inner diameter) placed in between the quartz plate and detector. All the surfaces of the cell components were gently polished and made plane-parallel with the thickness variation of about 2 μm to avoid possible distortions of the OA-signal profile due to a non-parallelism of the OA-source and detector surfaces. To perform an experiment, the OA-cell was filled with the test solution. The detector was made from a 28-μm PVDF film (Precision Acoustics) and operated in an open-circuit mode [48]. The detector was calibrated in the frequency range of 0.1–50 MHz and had a smooth spectral-transfer function in the range of 0.1–40 MHz and the low frequency sensitivity of 4.5 μV/Pa [44]. The detected OA-signals were amplified and digitized by a Tektronix TDS 1012 digital oscilloscope (USA; analog frequency, 100 MHz; sampling rate, 1 GHz).

2.1.3. Spectrophotometric measurements

The UV/Vis absorption spectra of solutions were registered on an Agilent Cary 60 spectrophotometer. The spectra were measured using quartz cells with an optical path length of 0.1 or 1 cm depending on the concentrations of the sample. All spectra were recorded from 190 to 1100 nm with a step of 1 nm and a scan rate of 600 nm/min. The ratio of spectra was obtained by dividing the absorbance of one sample by the absorbance of the another (limiting to the regions with absorbances of both solutions below 2.5 to reduce errors) at the same wavelength.

2.1.4. Other equipment

A Mettler DCS-30 TA instrument was used to capture heating traces from 233 up to 313 K. The scanning rates were 5 K/min. Each DSC sample weighed 15–20 mg.

TEM specimens were prepared by dispersing ND suspensions in ethanol onto TEM carbon–copper grids and by drying in vacuo (10^{-2} mm Hg). HRTEM imaging was performed with a JEM 2100 F transmission electron microscope with an accelerating voltage of 200 kV.

A CM-50 laboratory desktop centrifuge from ELMI Ltd. (a #50.01 rotor, 12 test-tubes of 0.2–2.0 mL, 1000–15000 rpm, RCF 15300*g* at r_{max} = 6.1 cm) and a Beckman L8-80 M ultracentrifuge (a 45Ti rotor for 6 test-tubes of 80 mL, 1000–50000 rpm) were used for fractionation.

A Kern 770 analytical balance was used for dry powder samples weighting. An Ecros 6500 shaker was used for the preparation of dispersions. A GRAD 28–35 ultrasound bath from Grad-Technology was used for preparing ND dispersions in water. A SNOL 20/300 heating oven (Snol-Term Ltd.) was used for the evaporation of ND aqueous dispersions. Automatic Eppendorf Research pipettes (Eppendorf International) were used for the preparation of calibration solutions. Polypropylene test tubes (Axygen) were used for solution preparation and storage.

2.2. Nanodiamond materials

Commercially available NDs were used throughout. Trademarks, their ID labels and manufacturers are listed in Table 1. All NDs are dry powders except SDND (already an aqueous dispersion). The aqueous dispersions were produced as reported elsewhere [22].

2.3. Other reagents

All the solutions were prepared with water from a Milli Q water purification system (Millipore; specific resistance, 18.2 MΩ × cm; Fe, 2 ppt; dissolved SiO_2, 3 ppb; total ion amount, < 0.2 ppb; TOC, below 10 ppb). The following reagents were used throughout: Phenol Red, $C_{19}H_{14}O_5S$ [CAS 143-74-8] (cp grade, MPBiomedicals) and *tris*(1,10-phenanthroline) iron(II) sulfate (ferroin) [CAS 14634-91-4] (Merck).

Table 1
Nanodiamonds used in the study.

NDs product name	Description	Manufacturer
RUDDM	modified ND material of RUDDM grade, fraction 0–150	Real-Dzerzhinsk Ltd., Russia
RDDM	modified ND material of RDDM grade, fraction 0–125	Real-Dzerzhinsk Ltd., Russia
SDND	single-digit NDs	PlasmaChem GmbH, Germany
NanoAmando	Dispersed single-ND particles NanoAmando (production year 2012)	NanoCarbon Research Institute Co., Ltd., Japan
UDA-GO-SP	deep purified ultradisperse diamonds	JSC SINTA, Belarus

2.4. Procedures

2.4.1. Preparation of ND dispersions in water

RUDDM (Table 1) powder (2.500 ± 0.001 g) was transferred to a volumetric flask (25.00 ± 0.08 mL), approx. 20 mL of deionized water was added. Next, it was subjected to 2 h of shaking followed by 0.5 h of ultrasonic treatment. Then, the flask was filled to the mark with deionized water and was subjected to 0.5 h of ultrasound treatment. RDDM powder (1.500/3.000 ± 0.001 g) was placed into a polypropylene test tube; next, 10.00 ± 0.12 mL of deionized water was added to the test tube, which was shaken for 2 h. The concentration of the stock solution was established gravimetrically. Other NDs are commercially available dispersions.

2.4.2. Preparation of ND solutions for spectrophotometry and optoacoustic studies of optically dense samples

If the stock solution was stored for more than one day before the preparation of working solutions, it was manually stirred vigorously. Then, a series of working solutions with concentrations 1–100 mg/mL for RUDDM and 0.7–140 mg/mL or 140–280 mg/mL for RDDM were prepared.

2.4.3. Centrifugation

A solution of RUDDM (100 mg/mL) was placed into 12 2-ml Eppendorf-type test-tubes, which then were centrifuged under 15000 rpm for 4 h. Next, 1 mL (fraction **1M**) and 0.5 mL (fraction **2M**) portions of the supernatant were taken in sequence from each test-tube. Both samples of the supernatant were collected in separate polypropylene tubes and concentrated by evaporating a part of water (concentrations were obtained gravimetrically after OA and UV/Vis studies). Fresh water was added to dissolve (1 h) the remaining sediments in test-tubes. The solutions were quantitatively moved into polypropylene test-tubes and evaporated in a heating oven. Then, the dry fraction was again dissolved (fraction **3M**).

2.4.4. Ultracentrifugation

A solution of RUDDM (100 mg/mL) was placed into two test-tubes (50 of 80 mL). Aqueous suspensions were centrifuged at 40000 rpm for 1 h. Then, 25 mL (pale light-brown fraction **1U**), 10 mL (light-brown fraction **2U**), 5 mL (brown fraction **3U**) portions of the supernatant were taken in sequence from each test-tube. Then, all three types of the supernatant were collected in separate polypropylene test-tubes and concentrated by evaporating a part of water (concentrations were obtained gravimetrically after OA and UV/Vis studies). Fresh water was added to dissolve (24 h) the sediments remaining in test-tubes. Obtained solutions were quantitatively moved into polypropylene test-tubes and evaporated in a heating oven. Then, the dry fraction was again dissolved (fraction **4U**).

2.4.5. Centrifugation of ultracentrifugated nanodiamonds

A solution of fraction **4U** (100 mg/mL) prepared according to the procedure 2.4.4 was placed into 12 2-mL Eppendorf-type test-tubes, which then were centrifuged under 15000 rpm for 4 h. Next, 1 mL (fraction **4U-1M**) and 0.5 mL (fraction **4U-2M**) portions of the supernatant were taken in sequence from each test-tube. Then, both samples of the supernatant were collected in separate polypropylene tubes and concentrated by evaporating a part of water (concentrations were obtained gravimetrically after OA and UV/Vis studies). Fresh water was added to dissolve (1 h) the remaining sediments in test-tubes. Obtained solutions were quantitatively removed into polypropylene test-tubes and evaporated in a heating oven (fraction **4U-3M**).

2.4.6. Preparation of ND samples for DSC

A portion of a ND sample was mixed with distilled water in a 1:2 ratio to give a gel sample (ND and water). The minimum amount of ND material necessary for one run was 1 mg. The DSC procedure is described in detail elsewhere [49].

2.5. Data processing

The exponential leading edge of the OA signal resembles the in-depth distribution of laser fluence in the solution and makes it possible to measure the absorption-coefficient changes very precisely

$$\log U = a + bt \tag{1}$$

where U is an OA-signal (Volts), a is a constant, $b = \mu_a c_0$, c_0 is the speed of sound, and μ_a is the light absorption coefficient. Fitting the slope with a linear function is used to obtain the coefficient μ_a. Finally, to build a calibration curve, absorbance was calculated as $A = \mu_a l/2.303$, where l is the thickness of the cylindric cell (4.9 mm).

The speed of sound c_0 in the solution was measured experimentally by the difference Δt in between arrival times of the primary OA-signal and its reverberation within the measurement cell with a optical path (thickness) length of l [50]. In this case, it is equal to $2l/\Delta t$. The relative error of speed-of-sound measurements was lower than 0.5%. An aqueous solution (5 mg/mL) of Phenol Red was added to increase the signal for calculating the speed of sound in water; the speed of sound in aqueous ND dispersions were measured without any additives.

Ultrasound attenuation α_{us} was measured by the detection of signals of the same solution in OA cells of different thickness

$$\alpha_{us} = \frac{\ln(S_2/S_1)}{l_1 - l_2} \tag{2}$$

where S_1 and S_2 are intensities of OA-signals recorded for cell thicknesses l_1 and l_2, respectively.

All the measurement results were processed in accordance with the requirements of ISO/IEC 17025:2005 [51] and IUPAC 1998 recommendations for the presentation of the results of chemical analysis [52]. The procedures were characterized by the repeatability relative standard deviation (RSD), and the minimum values of this error curve was used as another metrological parameter. To determine the significance of contributions to the signal of the control experiments, the series were compared by Student's *t*-test, and variances were compared using the Fisher test.

DSC was used as a method allowing to compare the sizes of diamond nanoparticles in various materials and to monitor the change in particle size during the separation of samples and to estimate their absolute size using the Gibbs–Kelvin equation [34,53]

$$\Delta T = \frac{4V_{mol}\sigma_{l\to s}T_m}{x\Delta H_m} \tag{3}$$

where $\sigma_{l\to s}$ is the surface tension at the liquid-solid interface [53], V_{mol},

T_m, and ΔH_m are the molar volume, the melting point (K), and the melting enthalpy of the bulk water, respectively [54], and x is the characteristic size of voids with the structured solvent. The values of x were previously shown to be close to the mean size of the nanodiamond particles forming the gel [34,49].

3. Results and discussion

The main problem for the analysis of NDs lies in their insoluble nature. However, NDs could be divided into two large groups [28]. The first group spontaneously forms finely dispersed colloids (hydrosols) without any ultrasound treatment even for high concentrations of the initial material — up to 10% wt. or even higher. These solutions are stable for a long time, and a very small amount of the precipitate appears with time. The second group contains a larger set of trademarks: these NDs cannot form a colloid solution without ultrasound treatment or form only suspensions with micrometer-scale particle size even after a long treatment. These suspensions are rather unstable, and precipitation begins 5–10 min after the ultrasound exposure [28]. In this study, as we focused on stable dispersions, we used NDs of the "soluble" group — SDND, RUDDM, RDDM, and NanoAmando trademarks and we selected UDA-GO-SP to test OA techniques on "insoluble" ND materials. All the "soluble" dispersions have the characteristic brownish yellow color, while UDA-GO-SP shows a grey color characteristic to scattering-dominated dispersions.

3.1. DSC measurements

Indirect measurement of diamond nanoparticle sizes by differential scanning calorimetry is based on the difference in the melting point of the bulk phase of the solvent in the dispersion and the solvent in the characteristic voids between diamond nanoparticles in the agglomerates [34]. The presence of two melting points changes the traditional form of a DSC curve (usually melting the bulk phase of a pure solvent shows a single peak) and the appearance of a second peak corresponding to a phase transition of the structured solvent at a lower temperature [53].

The temperature difference between two melting points for a pure solvent (water) and a water-containing nano-structured material, ΔT, Eq. (3) is accounted for the effective diameter of the voids filled by structured water. The larger ΔT is observed, the smaller are the voids, and the smaller the diameter of particles is [55]. This parameter is calculated directly from the experimental DSC traces, is characteristic for the test material, and is highly reproducible for NDs [34]. The value of ΔT in the case of nano-sized diamond does not depend on the method of preparation of ND-water mixtures (simple mixing, ultrasonic treatment, and the addition of water through the vapor phase) and the amount of water in the mixture. It is shown that the functional groups on the surface of diamond nanoparticles do not affect the value of ΔT [34].

We checked the size differences between different types of NDs by this approach previously [34] and obtain the data for other trademarks used in this study (Table 2). The correlation between ΔT and DLS size distribution was observed, also previously obtained XRD data for the smallest fractions and starting material agreed with DSC parameters

Table 2
DSC parameters of different NDs and temperature differences between the peaks and estimated mean particle sizes ($P = 0.95$, $n = 3$).

Trademark	ΔT, °C	Mean particle diameter
SDND [34]	9.2 ± 0.3	7.3 ± 0.5
NanoAmando [34]	8.2 ± 0.3	8.3 ± 0.5
UDA-GO-SP	< 2	> 40
RUDDM (this work)	7.3 ± 0.5	9.2 ± 0.5
RDDM (this work)	2.6 ± 0.5	25 ± 1

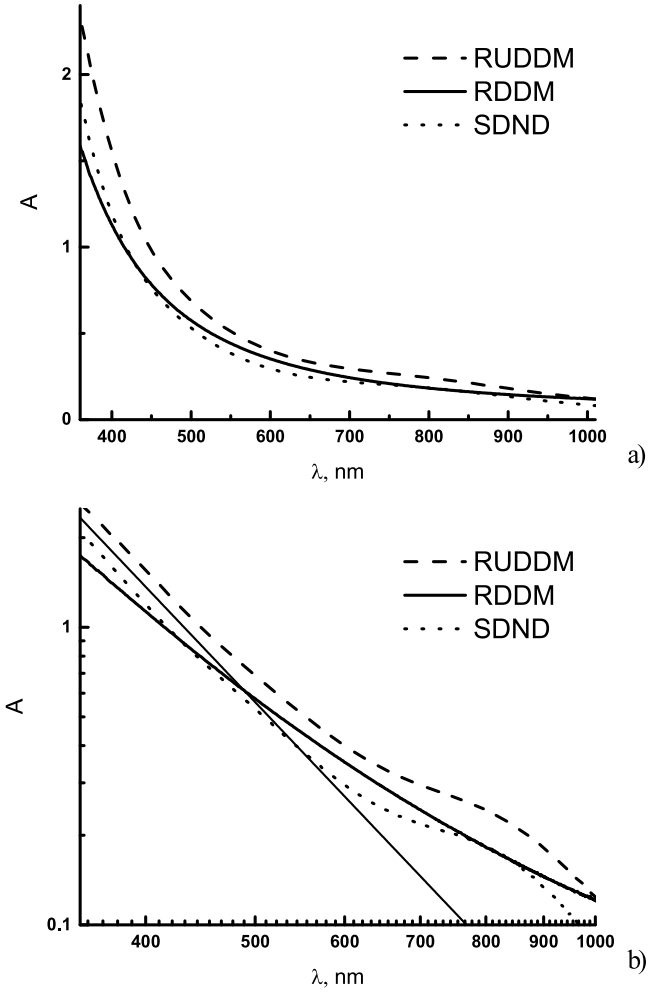

Fig. 1. Optical extinction spectra (a, a linear scale and b a log-log scale) of ND aqueous dispersions: RUDDM, 20 mg/mL (dashed line), SDND, 20 mg/mL (dotted line) and RDDM, 1.8 mg/mL (solid line). All results were normalized to the same optical path length of 1 mm. The theoretical Rayleigh scattering line λ^{-4} (thin solid line) is given for comparison.

[34]. According to this approach, SDND, RUDDM, and NanoAmando NDs have small particles of 7–9 nm, while RDDM, though highly soluble, has considerably larger particles of *ca.* 25 nm and has only two-fold lower size as an "insoluble" UDA-GO-SP material.

3.2. Optical extinction spectra of aqueous dispersions of nanodiamonds

UV/Vis spectra of the "soluble" ND dispersions are given in Fig. 1 and the data are summed up in Table 3. As shown previously [25,26,29], in UV and violet regions, absorbance should change as a function of λ^{-4} due to the strong and dominating Rayleigh scattering. The deviation of the ND absorbance spectrum from a λ^{-4} law depends

Table 3
Coefficients k of the equation $\log \mu = -k \log \lambda + b$ for the wavelength range 440–660 nm for conventional measurements and OA measurements for the ND trademarks ($P = 0.95$, $n = 3$).

Trademark	Optical absorption measurements	OA measurements
RDDM	2.80 ± 0.05	1.50 ± 0.05
RUDDM	3.20 ± 0.05	3.0 ± 0.1
SDND	3.30 ± 0.05	3.0 ± 0.1
UDA-GO-SP	2.1 ± 0.1	1.5 ± 0.1
NanoAmando	3.00 ± 0.05	2.5 ± 0.1

on nanodiamond purity and size [29]. The smaller particles are present, the higher absorption contribution is assessed [26]. For all "soluble" ND dispersions, we obtained linear dependences of $\log \mu = -k \log \lambda + b$, where in the range 300–450 nm the coefficient k is close to 4, which is consistent with previous data [25,26,29]. In the case of RDDM, however, it is difficult to find a region that obeys the λ^{-4} law in the UV/vis optical extinction spectrum (only for diluted to 1 mg/mL or lower concentrations).

In the range 400–600 nm, all "soluble" NDs show the slope of $\log \mu = -k \log \lambda + b$ from –3.2 to –2.8 (Table 3), which corresponds to an increased contribution from absorption due to the formation of Pandey chains or other surface groups [23,26,56], which start to contribute into the absorption properties of ND over 500 nm [27]. In the range of 800 nm, RUDDM, SDND, and NanoAmando NDs show distinct maxima of absorption, which correspond to the surface dimer absorption with a maximum at 1.5 eV [27]. High and similar slopes k for RUDDM, SDND, and NanoAmando could relate to smaller particles in these NDs.

As expected, the "insoluble" trademark, UDA-GO-SP, shows a linear $\log \mu = -k \log \lambda + b$ dependence with a slope of –2.1 in the whole range 300–1100 nm, and an almost indistinguishable maximum at 800 nm and a lower mass extinction coefficient is present. This can be considered an evidence of dominating scattering, taking into account the size of nanodiamond aggregates of 40 nm estimated for these species [34].

However, for most soluble NDs, RDDM, the absorption spectrum in the long-wave part is proportional to λ^{-2} and does not show the maximum of dimer chains similar to the highly scattering UDA-GO-SP (Fig. 1). In the same time, these NDs show a much higher mass-extinction coefficient than three other "soluble" trademarks, which is contradictory to the dominating scattering. Moreover, according to the elemental analysis of these ND samples [28], this trademark shows the minimum amount of elemental impurities, which may indirectly manifest a low degree of surface functionalization. The comparison with DSC data leads to a preliminary conclusion that RDDM is not a purely nanodiamond material, and its solubility may be governed by other carbon forms. Thus, in this sample, sp^2 carbon is probably the main component of non-ND impurities, rather than a shell on diamond core particles [39]. However, based on optical-absorption data only, it is difficult to conclude why this material is different from other "soluble" trademarks.

3.3. Optoacoustic spectra of aqueous dispersions of nanodiamonds

The development of optical parametric oscillators (OPO) as excitation sources opened up new possibilities for photothermal and optoacoustic spectroscopies and introduced multispectral measurements [46,57–60]. Multiwavelength (multispectral) optoacoustic techniques can be used for a more detailed comparison of optical-absorption and calorimetric spectra [61,62]. We used an OPO-based multiwavelength optoacoustic setup [46] for studying extinction spectra of aqueous dispersions of the selected ND types (Fig. 2). For the multispectral technique, we selected the measurements of ND solutions as very thin samples to maximally avoid the contribution from light scattering. The correctness of the spectra of OA measurements under these conditions was checked using ferroin as a dye giving true solutions, which showed only slight deviations from the optical-absorption spectra (Fig. S2, Supplementary information). The OA spectral range was limited by the working wavelength (410–710 nm) of the OPO used in the instrument. Low energy of excitation pulses for short and long wavelengths produced the noisy signals; thus, to avoid the artifacts; only the range 440–660 nm of OA spectra was treated. As this technique is highly sensitive, we measured the spectra for ND concentrations of 1–10 mg/mL in thin liquid layers. In this concentration range, the acoustic attenuation was negligible (Fig. 3).

The comparison of OA shows that the absorbances calculated from OA data significantly differ from spectrophotometry. The spectra

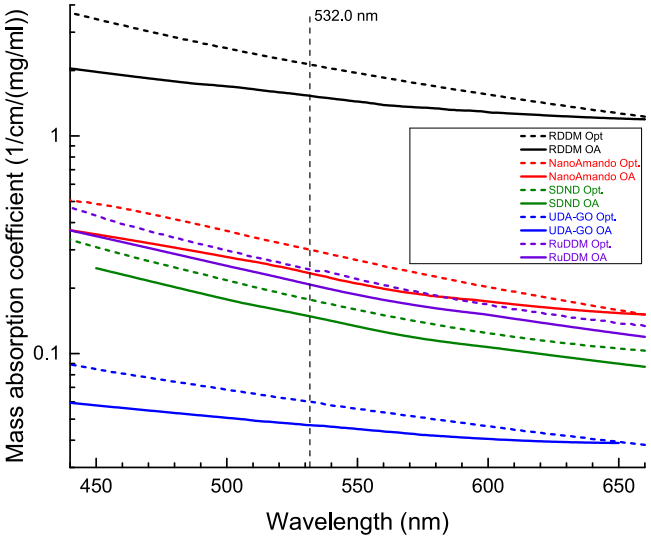

Fig. 2. Absorption spectra of ND obtained using conventional spectrophotometry (dotted lines) and calculated from optoacoustic measurements (solid lines, smoothing by Savitzky-Golay algorithm, 40 points) for 4 mg/mL solutions.

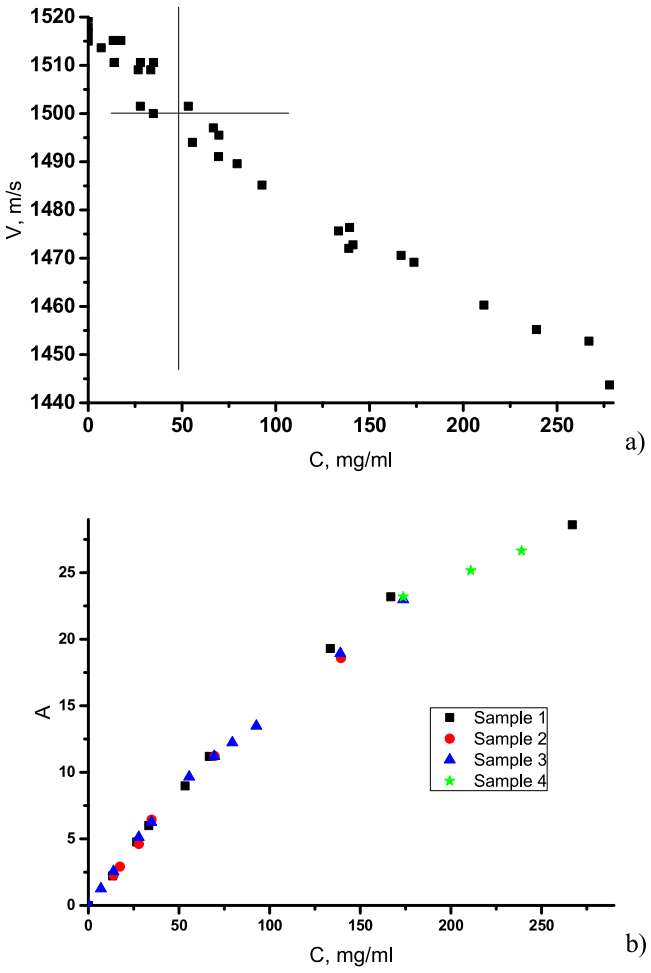

Fig. 3. The speed of sound a) and absorbance at 532 nm b) dependence on concentration of RDDM in aqueous dispersion, four different samples (different dates of measurements of the same solution).

showed shapes different from optical spectra, and the coefficients k of the equation $\log \mu = -k \log \lambda + b$ (Table 3) were lower compared to optical measurements. However, for RUDDM, SDND, and NanoAmando, the slopes decreased only slightly and a change in the mass extinction coefficient compared to spectrophotometry is 10–20%. The most drastic decrease in the absorption spectrum was observed for RDDM, the coefficient k decreased to the value of 1.5, which is the same as the OA coefficient for the "insoluble" UDA-GO-SP, which agrees well with the size of particles from DSC measurements (Section 3.1). Still, the mass extinction coefficient of RDDM from OA measurements is an order higher that for RUDDM, NanoAmando, and SDND materials. The mass absorption coefficients are in good agreement with the data for small-sized purified NDs [27] and are of the same order as meteorite-based NDs [33].

For all the samples, the most significant difference between OA and optoacoustic spectra was observed for shorter wavelengths at 450 nm. Within the error of experiment, the spectra were nearly coincident at wavelengths of 600–650 nm, which may be an evidence of the dominating nature of absorption of surface dimer Pandey chains into the total extinction signal. While for UV/Vis spectroscopy, the deviation from a pure λ^{-x} dependences becomes significant at wavelengths over 650 nm (Fig. 1, see also the data in [27]), in OA spectra less prone to Rayleigh scattering, this effect appears at wavelength over 600 nm (even 570 nm for NanoAmando and RDDM materials). This is coincident with the calculations of the high energy edge of the absorption band in ND due to the transitions between surface states of 2.1 eV [27].

As the OA modality is much less dependent on Rayleigh light scattering compared to spectrophotometry [45,50,63–65], such a correlation of OA and conventional spectra can reveal that the spectra of nanodiamonds are mainly governed by light absorption. This is in concordance with the high sensitivity of photothermal-lens determination of ND aqueous dispersions in the visible range (comparable to highly absorbing substances in water) [22], as photothermal-lens measurements also show only a slight effect of Rayleigh scattering. Thus, the difference of OA and optical-absorption spectra may be used, as the first approximation, for estimating the contributions of the scattering and absorption to the extinction spectra of NDs.

For UDA-GO-SP, the large contribution of scattering was observed, as expected. Still the absorption was found and the same increase in the range over 550 nm was found as for "soluble" trademarks. It is interesting that highly soluble RDDM ND shows approximately the same difference between OA and optical extinction spectra. For three other trademarks, the difference between OA and optical extinction spectra is almost the same in shape and values. The comparison of spectra for RDDM and other aqueous dispersions (RUDDM, NanoAmando, and SDND) shows that RDDM NDs have both higher light-scattering as well as higher light absorption, which confirms the conclusion of significantly different purity grades of these materials. Thus, OA spectra also show that RDDM NDs have large and impure particles at the same time, but a better solubility.

The OA spectra of NDs allowed us to make a more detailed study of NDs for concentrated solutions using the OA technique for optically dense solutions.

3.4. Optoacoustic and UV/vis data comparison for concentrated nanodiamond samples

The general possibilities and the theoretical basis of the OA technique for optically dense samples in applied chemistry were shown [44,66,67]. The advantage of this technique is that it provides the reliable information on the light absorption coefficients against large light-scattering coefficients [45,65]. It is used for measurements of laser fluence distribution [44,66,67] and found application in physico-chemical and biological studies [61,68–73]. This technique was applied to study the absorption at 532 nm of ND dispersions. Only two ND types—RDDM and RUDDM—were selected for this part of the study as they share the same production protocol, form highly concentrated solutions with sufficient absorption at 532 nm (Fig. 2) and, as we showed in the previous sections, are characterized by significantly different spectra and other properties.

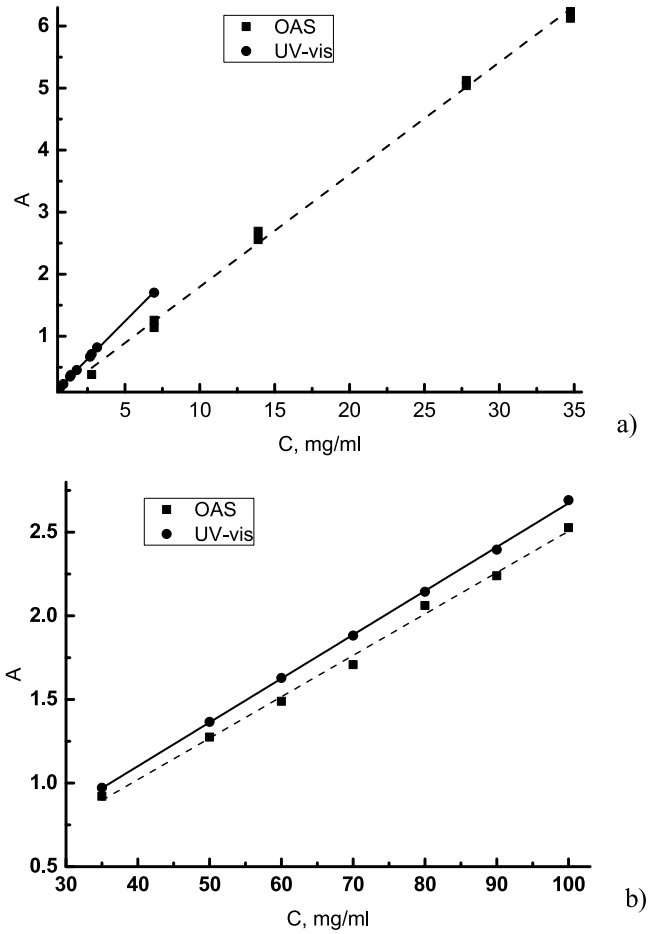

Fig. 4. Calibration curves (532 nm) for RDDM a) and RUDDM b) from UV/vis and OA measurements. All results were normalized to the same thickness of 1 mm.

Fig. 4 presents calibration curves for RDDM and RUDDM aqueous dispersions from optoacoustic and spectrophotometric measurements. The OA technique allows determining absorbances even for very concentrated solutions (up to 280 mg/mL, see Fig. S3, Supplementary information). As we see, multispectral OA measurements showed that for RUDDM, the extinction at 532 nm is dominated by absorption (Fig. 2), and both methods give similar results (Table 4). The slopes from the setup are in good concordance with the values of mass absorption coefficients from OA spectra. As for RDDM aqueous dispersions, the difference in slopes is significant because of a large scattering part (Fig. 2) which increases UV/vis signals and does not influence on optoacoustic measurements. The extinction coefficient of RDDM is about an order of magnitude greater than for RUDDM. The mass absorption coefficients for both OA techniques agree within the error of measurements for both aqueous dispersions.

The speed of sound of ND aqueous dispersions was checked for

Table 4
Slopes (mL/mg) of calibration curves for different NDs ($P = 0.95$, $n = 7$–9).

Trademark	UV/vis	OA
RUDDM	$(2.62 \pm 0.05)\cdot10^{-2}$	$(2.5 \pm 0.2)\cdot10^{-2}$
RDDM	$(2.4 \pm 0.1)\cdot10^{-1}$	$(1.8 \pm 0.1)\cdot10^{-1}$

RDDM for concentrations up to 280 mg/mL. These solutions are not acoustically transparent, and the speed of sound is decreased significantly for concentrations above 40 mg/mL (Fig. 3). Slope of calibration curve changes with an increase in the concentration of NDs over 60 mg/mL, it may be accounted for a significant increase in viscosity of concentrated ND solutions [24].

A detailed investigation of this effect may be the scope of another research, and here we just state that the used OA technique broadens the concentration range of ND determination by optical spectroscopy. It should be noted that other techniques allowing to retrieve the individual contributions from light scattering and light absorption can be used for further elucidation of the extinction spectra of nanodiamonds like the photoacoustics modality in a frequency mode with the Kubelka–Munk theory as recently shown by the case of ZnO nanoparticles on diatom surfaces [74,75].

3.5. Nanodiamond fractionation

Fractionation of NDs was investigated previously [25,26,29,34–42,76]. However, optical spectra of different fractions have not been considered in detail. Previously, it was found that non-diamond carbon could be removed from ND fractions [39] and the fractions have different surface chemical composition and therefore physicochemical properties [40,76], which apparently may affect the optical properties. Thus, we used centrifugation to see in more detail how the UV/vis spectrum and absorption at 532 nm by OA measurements depend on fraction size and composition. Dealing with fractions, we used both methods (UV/vis and the OA technique for optically dense samples) and applied DSC for monitoring the size change [34]. To test the possibility of centrifugation, we use both centrifugation (acceleration of gravity of 15000*g*) and ultracentrifugation (130000*g*).

After ordinary centrifugation (Procedure 2.4.3), we obtained two supernatant fractions, upper (1 mL, named **1M**) and lower (0.5 mL, **2M**). The rest of nanodiamonds was collected as a dry fraction and dissolved (fraction **3M**). As expected, fractions after centrifugation at 15000 rpm consist of particles of various sizes: the uppermost fraction has the smaller size of 3.6 nm, which is coincident with previous findings [76], the second fraction has the size of 5.2 nm, while the bottommost fraction has the same size as the starting materials (Table 5). The most interesting is the upper fraction, **1M**. This fraction is sedimentation-unstable. According to Fig. 5, **1M** fraction possesses higher light absorption especially at long wavelengths, which may be an evidence of a ND fraction with surface dimer chains. However, the absorption spectrum shows a lower relative absorption at longer wavelengths and the absorbance ratio spectrum does not show a characteristic peak at 800 nm (1.5 eV) corresponding to the transitions between levels of the surface forbidden zone. Thus, such a change in the spectrum could be assigned to the enrichment with non-diamond sp^2 carbon in this fraction. To clarify this, we subjected RUDDM to the ultracentrifugation.

Table 5
DSC parameters for fractions after centrifugation, ultracentrifugation, and subsequent centrifugation of the bottommost ultracentrifugated fraction and estimated mean particle sizes ($P = 0.95$, $n = 3$).

Fraction	ΔT, °C	Mean particle diameter
Starting RUDDM	7.3 ± 0.5	9.2 ± 0.5
1M	19.4 ± 0.3	3.6 ± 0.4
2M	13.3 ± 0.3	5.2 ± 0.5
3M	6.9 ± 0.5	9.7 ± 0.5
1U	19.8 ± 0.3	3.6 ± 0.4
2U	19.0 ± 0.3	3.7 ± 0.4
3U	19.5 ± 0.3	3.6 ± 0.4
4U	6.7 ± 0.5	10.0 ± 0.5
4U-1M	20.1 ± 0.3	3.5 ± 0.4
4U-2M	15.2 ± 0.3	4.6 ± 0.5
4U-3M	6.8 ± 0.5	9.9 ± 0.5

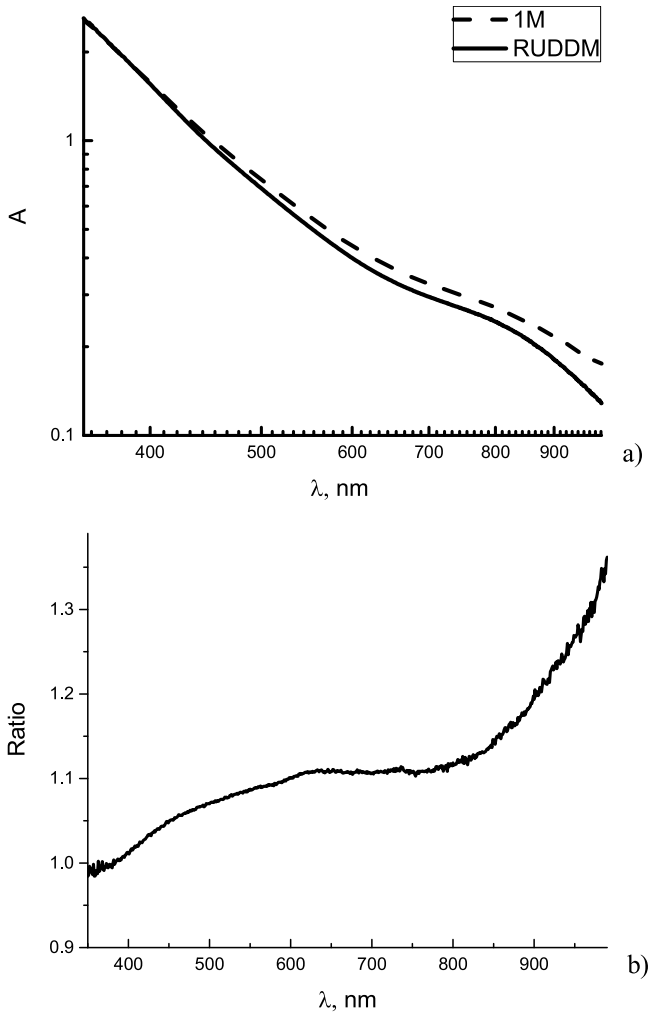

Fig. 5. The comparison of UV/vis spectra of the highest supernatant fraction (**1M**, 18.9 mg/mL) and the starting RUDDM solution (20.0 mg/mL) a) UV/Vis spectrum; b) absorbance ratio spectra of the **1M** fraction to the starting RUDDM material.

3.5.1. Ultracentrifugation

Ultracentrifugation is a commonly used method for ND fractioning, basically for improving the stability [35,37,38]. FTIR was used to demonstrate different surface compositions of fractions characterized by different particle sizes [35]. We conducted the experiment in a different way (Procedure 2.4.4), using almost the maximum possible speed (up to 40000 rpm) for a long time (1 h) and another way of distinguishing fractions.

After processing the initial RUDDM (100 mg/mL), we separated three supernatants: 25 mL, pale light-brown (**1U** fraction), 10 mL, light-brown, (**2U** fraction), and 5 mL (brown, **3U** fraction). As in the previous section, the rest of nanodiamonds was collected as a dry fraction and dissolved (**4U** fraction). Usually, for such separation, a sequential increase of the *g*-factor in a single run is applied (multi-step); however, we separated fractions from the same supernatant by sequential sampling. According to DSC, all three upper fractions have particles with the same small size of 3.6 nm, while the bottommost fraction has a slightly increased mean size compared to the starting material (Table 5). Fig. S4 (Supplementary information) shows typical DSC traces for several fractions and the starting material.

Interestingly, these fractions have different UV/vis spectra. As seen from Fig. 6, a, upper fractions have spectra untypical for ND aqueous

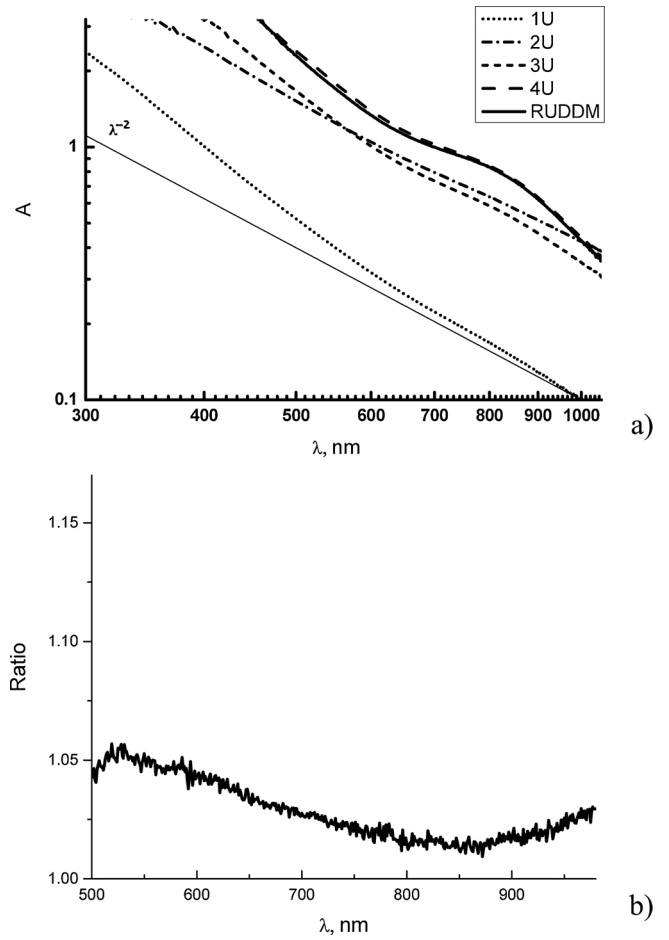

Fig. 6. a) Optical extinction spectra (log-log) of fractions after ultracentrifugation (7, 13.2, 28, 72.5 mg/mL for **1U**, **2U**, **3U**, and **4U,** respectively) and the starting RUDDM material (70 mg/mL). b) The absorbance ratio of spectra of the **4U** fraction and starting RUDDM material.

dispersions (Fig. 1). Absorbance of the **1U** fraction changes approximately as a function of λ^{-3} in UV and violet regions and in the NIR region it can be described as λ^{-x}, $2 < x < 3$, which is different from the strict behavior of λ^{-4} of the starting material. These data are consistent with assumption that the removal of large particles decrease the scattering intensity in a radical way [26] and if light is absorbed by sp^2 carbon, the absorbance can be represented by a λ^{-2} dependence [23]. Water evaporation from **1U** and **2U** fractions gives particles with poor solubility in water, but the pellet (**4U** fraction) has a higher solubility than the starting RUDDM. It is possible to obtain dispersions with concentrations up to 200 mg/mL. It agrees well with the assumption that during ultracentrifugation upper fractions are enriched with the sp^2 phase.

HRTEM images of the **1U** fraction are presented in Fig. 7. It is difficult to distinguish particles because they are very small and have a polyhedral nature, which shows that this is not the diamond fraction; all the images are quite similar. The size of each crystallite is about 2–6 nm, which agrees well with the mean size estimation using DSC (Table 5) 1.7 Å distances between the lines (green straight lines in Fig. 7, b) corresponding to the graphite lattice spacing (d_{002} = 3.37 Å, ASTM C558-65 T, 1967) are clearly observed in all images; diamond structures are not seen, which is contradictory to the findings [76] when the authors claim to obtain the pure ND fractions by ultracentrifugation. However, our results are in concordance with the absorption spectrum of the 1U fraction (Fig. 6, a) showing a dependence with no distinct features at 300 and 800 nm with λ^{-3} for shorter and λ^{-2} for longer wavelengths, which also reveals no ND phase.

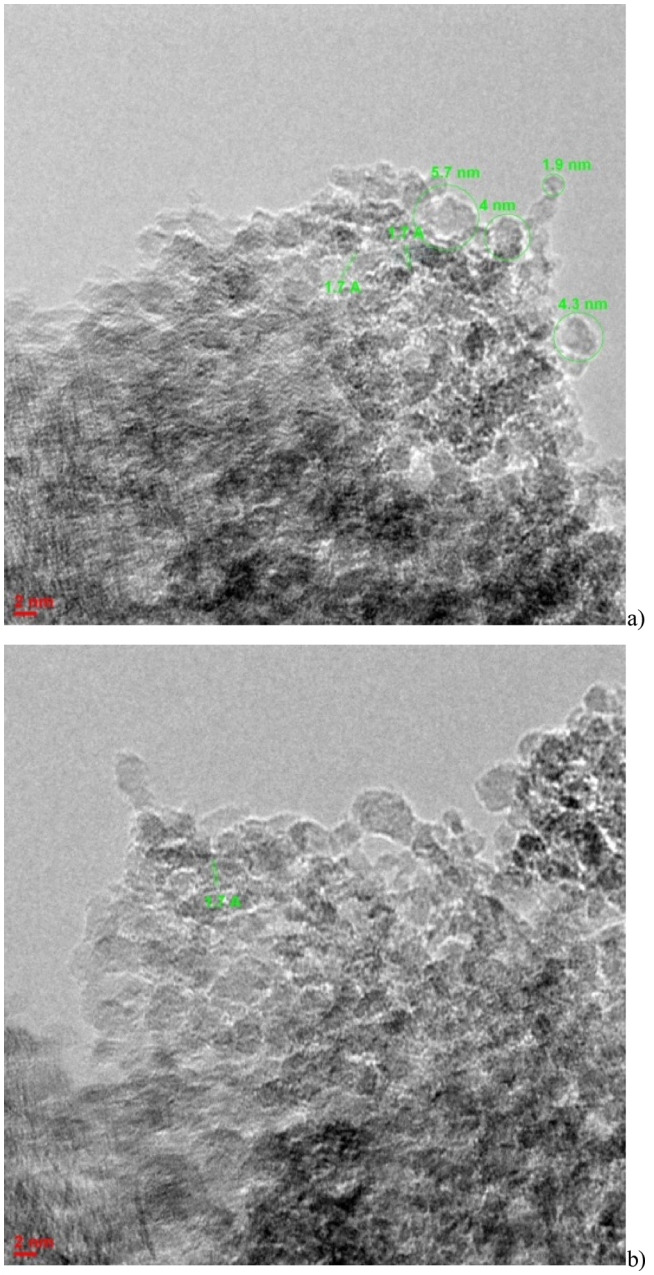

Fig. 7. HRTEM of the RUDDM fraction **1U** after 4 h of ultracentrifugation showing a) polyhedral graphite particles b) distance corresponding to the graphite lattice spacing.

Fractions **2U** and **3U** are very similar in spectra (Fig. 6, a), behavior, and the estimated mean size (Table 5) to fraction **1M**. They also should be considered as governed by sp^2 carbon absorption, with a ND-enriched fraction in **3U**, according to the spectra.

The bottommost **4U** fraction (sediment) after ultracentrifugation has a surprisingly better solubility compared to the starting RUDDM, but it has mainly the same mean particle size (Table 5) as the starting material and has the same UV/vis spectrum (Fig. 6, a). The absorbance-ratio spectrum for **4U** fraction and the starting RUDDM only slightly deviates from the horizontal line and the ratio of 1:1 in the range 800–900 nm (Fig. 6, b).

3.5.2. *Extra centrifugation of the bottommost ultracentrifugated fraction*

The solution of fraction **4U** (100 mg/mL) prepared by ultracentrifugation was additionally centrifuged under 15000 rpm for 4 h

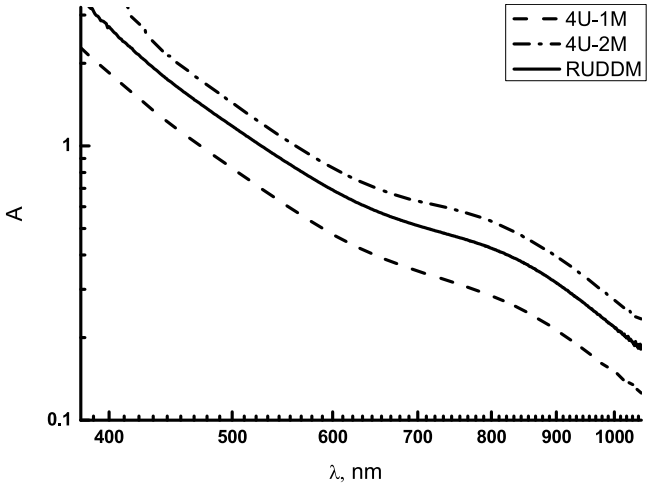

Fig. 8. UV/vis spectra (log-log) of fractions after microcentrifugation (23 and 46.3 mg/mL for **4U-1M** and **4U-2M**, respectively and the starting RUDDM material (35 mg/mL).

and separated similarly to the initial ND material (Procedure 2.4.5): two supernatant fractions, upper (1 mL, **4U-1M**) and lower (0.5 mL, **4U-2M**) were separated. The rest of the material was gathered as the **4U-3M** fraction. At this stage, we show trends of curves rather than perform a detailed intensity comparison.

This second centrifugation of the bottommost fraction resulted in yet another fraction with the size of 3.5 nm (Table 5). And, to the contrary of centrifugation or ultracentrifugation alone, this uppermost fraction has extinction spectra typical for nanodiamonds, with all the characteristic features (Fig. 8). It leads us to conclude that non-diamond sp^2 phase is mostly separated during the ultracentrifugation and after the second step, we get the real small-size ND fraction.

3.5.3. Optoacoustic and UV/vis data comparison for ultracentrifugated nanodiamonds

The alteration in the size and composition during the centrifugation and ultracentrifugation fractionation significantly affects the optical properties of ND aqueous dispersions. This can be shown by the comparison of highly concentrated solutions of ND powders gathered after the fractionation and the comparison with the original calibrations.

As seen from optical UV/vis spectra (Fig. 9, a), fractions **3U** and **3M** (the pellet after ordinary centrifugation) have rather high absorbances, while other fractions do not deviate from the main calibration. The **3U** fraction as well as **1U** and **2U** consists of small particles (Table 5) and feasibly contains some higher amounts of the non-diamond sp^2 phase compared to the starting RUDDM material. An increase in **3M** absorbance might relate to different scattering of starting RUDDM (consists of various types of particles) and **3M** fraction — as the pellet after centrifugation, it does not include small particles.

Absorbances of fractions estimated using the OA technique are influenced to a higher degree by the different size and composition of particles. Contrary to optical extinction measurements, all the fractions are different from the calibration curve of the starting RUDDM (Fig. 9, b). Here, the fractions, which were proven mainly non-diamond (**1M**, **1U**, and **2U**) were discarded, and only fractions with spectra with distinct ND features are shown. This figure shown that centrifugation alone (**2M** and **3M**) and ultracentrifugation alone (**3U** and **4U**) provide more absorbing fractions, but as we shown above, these is not the concentration of NDs but still non-diamond enriched fractions. And only the two-step fractionation provided fractions with all the features of NDs and lower absorption as most sp^2 carbon was removed and the absorption is governed most probably by Pandey dimer chains on the surface. Thus, the main light-absorbing layer of ND can be separated by a combination of centrifugation and ultracentrifugation, also producing

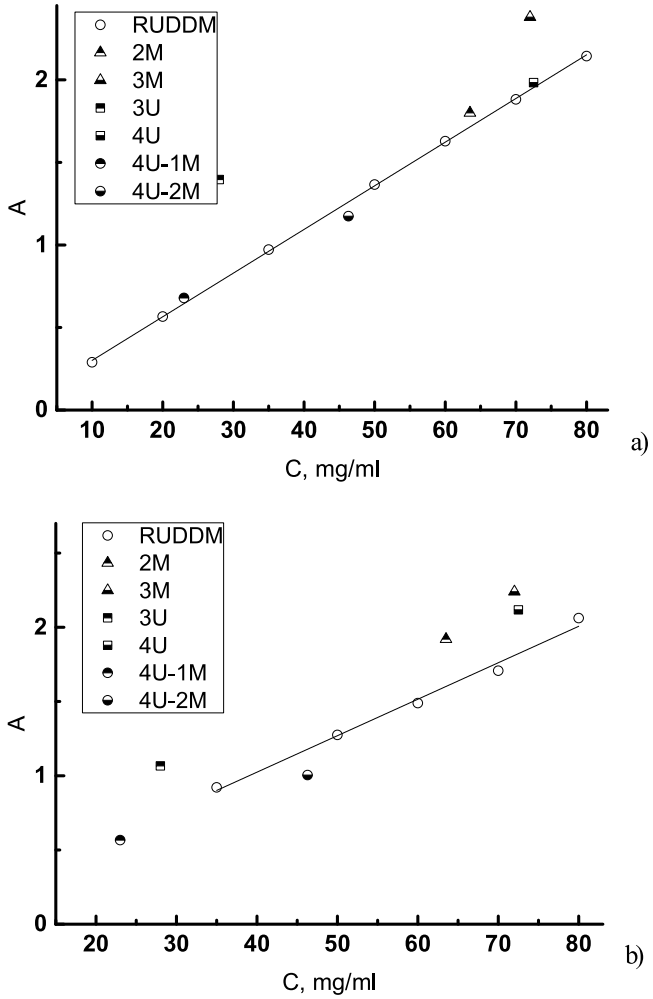

Fig. 9. Calibration curves for starting RUDDM and absorbances of several fractions (triangles, squares and circles for fractions after microcentrifugation, ultracentrifugation and ultra-microcentrifugation) obtained from a) optical extinction and b) OA techniques.

the bottommost fraction of ND, which has a higher solubility than the starting material.

To conclude, the comparison of the absorbances of solutions of fractions (with the same concentration) with the data of DSC and X-ray diffraction obtained previously [34] is rather indicative as well (Fig. S5, Supplementary information). The results correlate well with each other, which is quite unexpected, given the completely different nature of the analytical signals on the one hand, and the structural levels of the colloidal ND solutions, on the other. Nevertheless, it is quite clear that particles with a smaller size of coherently scattering domains in XRD give solutions with smaller aggregates and a lower absorption (i.e., with a lower contribution of light scattering, and, hence, again with a smaller aggregate size).

4. Conclusions

Thus, optoacoustic spectroscopy along with optical absorption techniques was applied to testing manufactured detonation nanodiamonds to provide a larger volume of reliable information on light absorption and scattering of samples compared to conventional techniques. The possibility of multiwavelength (multispectral) OA-technique to complement conventional spectrophotometric data on the nature of extinction spectra of nanodiamond aqueous dispersions, previously unimplemented, seems rather relevant. It can be used not only for NDs,

but with other carbon nanomaterials like fullerenes, nanotubes, or other dispersions of various nature to get more information on real light absorption of these materials, light-scattering contribution, and the photothermal effects to the overall picture of their properties. This seems even more relevant for biological applications of carbon nanomaterials when the extinction of the natural backgrounds may have a very complex nature.

The findings by the multispectral modality were supported by the OA technique for optically dense solutions, which were used for further elucidation of the contribution of scattering and absorption into the signals. To further advance the optoacoustic techniques, a much larger scale of studies is required for a wide set of samples. The techniques used in this study may be implemented with other OA modalities for separate contribution from light absorption and light scattering [74,75].

The important, previously unrealized, feature is the comparison on a series of ND samples by essentially different methods of analysis and research. This comparison made it possible to reveal rather not obvious but useful regularities, in even more cases, to raise new questions which, for the most relevant problems of nanodiamond applications, will require further research. This comparison was also confirmed by the fractionation experiments that revealed the separation of differently absorbing fractions with dominating graphite-like sp^2 carbon fractions and slightly surface-absorbing nanodiamond fractions. Still, the problem of the theoretical description of the fact that diamonds insoluble in water with a decrease in size to nanometers suddenly begin to behave like an ionic substance, spontaneously forming highly concentrated solutions, stable for many years, remains unresolved.

Conflict of interest

None.

Acknowledgments

This study was supported by the Russian Foundation for Basic Research [grants nos. 16-33-60147 mol_a_dk and 18-33-00586 mol_a].

Appendix A. Supplementary data

Supplementary material related to this article can be found, in the online version, at doi:https://doi.org/10.1016/j.pacs.2018.10.003.

References

[1] O.V. Turova, E.V. Starodubtseva, M.G. Vinogradov, V.I. Sokolov, N.V. Abramova, A.Y. Vul, A.E. Alexenskiy, Palladium supported on detonation nanodiamond as a highly effective catalyst of the C = C and C C bond hydrogenation, Catal. Commun. 12 (7) (2011) 577–579.
[2] N.N. Vershinin, O.N. Efimov, V.A. Bakaev, A.E. Aleksenskii, M.V. Baidakova, A.A. Sitnikova, A.Y. Vul, Detonation nanodiamonds as catalyst supports, Fuller. Nanotub. Carbon Nanostruct. 19 (1-2) (2011) 63–68.
[3] V.S. Bondar, I.O. Pozdnyakova, A.P. Puzyr, Applications of nanodiamonds for separation and purification of proteins, Phys. Sol. State 46 (4) (2004) 758–760.
[4] S.-Y. Wu, W.-M. Chang, H.-Y. Tseng, C.-K. Lee, T.-T. Chi, J.-Y. Wang, Y.-W. Kiang, C.C. Yang, Geometry for maximizing localized surface plasmon resonance of Au nanorings with random orientations, Plasmonics 6 (3) (2011) 547–555.
[5] N.A. Skorik, A.L. Krivozubov, A.P. Karzhenevskii, B.V. Spitsyn, Physicochemical study of the nanodiamond surface, Prot. Met. Phys. Chem. Surf. 47 (1) (2011) 54–58.
[6] G.P. Bogatyreva, M.A. Marinich, V.L. Gvyazdovskaya, Diamond — an adsorbent of a new type, Diam. Relat. Mater. 9 (12) (2000) 2002–2005.
[7] H.-D. Wang, C.H. Niu, Q. Yang, I. Badea, Study on protein conformation and adsorption behaviors in nanodiamond particle-protein complexes, Nanotechnology 22 (14) (2011).
[8] D. Ho, Nanodiamonds: Applications in Biology and Nanoscale Medicine, Springer, New York, Dordrecht, Heidelberg, London, 2010, p. 304.
[9] K. Turcheniuk, N.M. Vadym, Biomedical applications of nanodiamond (review), Nanotechnology 28 (25) (2017) 252001.
[10] B.R. Smith, D.W. Inglis, B. Sandnes, J.R. Rabeau, A.V. Zvyagin, D. Gruber, C.J. Noble, R. Vogel, E. Osawa, T. Plakhotnik, Five-nanometer diamond with luminescent nitrogen-vacancy defect centers, Small 5 (14) (2009) 1649–1653.
[11] N. Mohan, Y.-K. Tzeng, L. Yang, Y.-Y. Chen, Y.Y. Hui, C.-Y. Fang, H.-C. Chang, Sub-20-nm fluorescent nanodiamonds as photostable biolabels and fluorescence resonance energy transfer donors, Adv. Mater. 22 (7) (2010) 843–847.
[12] N. Mohan, C.-S. Chen, H.-H. Hsieh, Y.-C. Wu, H.-C. Chang, In vivo imaging and toxicity assessments of fluorescent nanodiamonds in caenorhabditis elegans, Nano Lett. 10 (9) (2010) 3692–3699.
[13] M. Chen, X.-Q. Zhang, H.B. Man, R. Lam, E.K. Chow, D. Ho, Nanodiamond vectors functionalized with polyethylenimine for siRNA delivery, J. Phys. Chem Lett. 1 (21) (2010) 3167–3171.
[14] M. Chen, E.D. Pierstorff, R. Lam, S.-Y. Li, H. Huang, E. Osawa, D. Ho, Nanodiamond-mediated delivery of water-insoluble therapeutics, ACS Nano 3 (7) (2009) 2016–2022.
[15] V.N. Mochalin, O. Shenderova, D. Ho, Y. Gogotsi, The properties and applications of nanodiamonds, Nat. Nanotechnol. 7 (1) (2012) 11.
[16] L. Moore, J. Yang, T.T.H. Lan, E. Osawa, D.-K. Lee, W.D. Johnson, J. Xi, E.K.-H. Chow, D. Ho, Biocompatibility assessment of detonation nanodiamond in non-human primates and rats using histological, hematologic, and urine analysis, ACS Nano 10 (8) (2016) 7385–7400.
[17] M. Avdeev, N. Rozhkova, V. Aksenov, V. Garamus, R. Willumeit, E. Osawa, Aggregate structure in concentrated liquid dispersions of ultrananocrystalline diamond by small-angle neutron scattering, J. Phys. Chem. C 113 (22) (2009) 9473–9479.
[18] O.V. Tomchuk, D.S. Volkov, L.A. Bulavin, A.V. Rogachev, M.A. Proskurnin, M.V. Korobov, M.V. Avdeev, Structural characteristics of aqueous dispersions of detonation nanodiamond and their aggregate fractions as revealed by small-angle neutron scattering, J. Phys. Chem. C 119 (1) (2014) 794–802.
[19] A. Krueger, D. Lang, Functionality is key: recent progress in the surface modification of nanodiamond, Adv. Funct. Mater. 22 (5) (2012) 890–906.
[20] S. Kidalov, F. Shakhov, A.Y. Vul, Thermal conductivity of sintered nanodiamonds and microdiamonds, Diam. Relat. Mater. 17 (4-5) (2008) 844–847.
[21] B.T. Branson, P.S. Beauchamp, J.C. Beam, C.M. Lukehart, J.L. Davidson, Nanodiamond nanofluids for enhanced thermal conductivity, ACS Nano 7 (4) (2013) 3183–3189.
[22] D.S. Volkov, P.I. Semenyuk, M.V. Korobov, M.A. Proskurnin, Quantification of nanodiamonds in aqueous solutions by spectrophotometry and thermal lens spectrometry, J. Anal. Chem. (Russ.) 67 (10) (2012) 842–850.
[23] E.D. Eidelman, V.I. Siklitsky, L.V. Sharonova, M.A. Yagovkina, A.Y. Vul, M. Takahashi, M. Inakuma, M. Ozawa, E. Osawa, A stable suspension of single ultrananocrystalline diamond particles, Diam. Relat. Mater. 14 (11-12) (2005) 1765–1769.
[24] A.Y. Vul, E. Eydelman, M. Inakuma, E. Ōsawa, Correlation between viscosity and absorption of electromagnetic waves in an aqueous UNCD suspension, Diam. Relat. Mater. 16 (12) (2007) 2023–2028.
[25] A.Y. Vul, E. Eydelman, L. Sharonova, A. Aleksenskiy, S. Konyakhin, Absorption and scattering of light in nanodiamond hydrosols, Diam. Relat. Mater. 20 (3) (2011) 279–284.
[26] A. Aleksenskii, A.Y. Vul, S. Konyakhin, K. Reich, L. Sharonova, E. Eidel'man, Optical properties of detonation nanodiamond hydrosols, Phys. Sol. State 54 (3) (2012) 578–585.
[27] A.E. Aleksenskii, A.Y. Vul', S.V. Konyakhin, K.V. Reich, L.V. Sharonova, E.D. Eidel'man, Optical properties of detonation nanodiamond hydrosols, Phys. Sol. State 54 (3) (2012) 578–585.
[28] D.S. Volkov, M.A. Proskurnin, M.V. Korobov, Elemental analysis of nanodiamonds by inductively-coupled plasma atomic emission spectroscopy, Carbon 74 (2014) 1–13.
[29] O. Shenderova, V. Grichko, S. Hens, J. Walch, Detonation nanodiamonds as UV radiation filter, Diam. Relat. Mat. 16 (12) (2007) 2003–2008.
[30] W.W.W. Hsiao, Y.Y. Hui, P.-C. Tsai, H.-C. Chang, Fluorescent nanodiamond: a versatile tool for long-term cell tracking, super-resolution imaging, and nanoscale temperature sensing, Acc. Chem. Res. 49 (3) (2016) 400–407.
[31] H. Eidi, M.-O. David, G. Crépeaux, L. Henry, V. Joshi, M.-H. Berger, M. Sennour, J. Cadusseau, R.K. Gherardi, P.A. Curmi, Fluorescent nanodiamonds as a relevant tag for the assessment of alum adjuvant particle biodisposition, BMC Med. 13 (1) (2015) 144.
[32] S.R. Hemelaar, P. de Boer, M. Chipaux, W. Zuidema, T. Hamoh, F.P. Martinez, A. Nagl, J.P. Hoogenboom, B.N.G. Giepmans, R. Schirhagl, Nanodiamonds as multi-purpose labels for microscopy, Sci. Rep. 7 (1) (2017) 720.
[33] H. Mutschke, A.C. Andersen, C. Jäger, T. Henning, A. Braatz, Optical data of meteoritic nano-diamonds from far-ultraviolet to far-infrared wavelengths *, A&A 423 (3) (2004) 983–993.
[34] M.V. Korobov, D.S. Volkov, N.V. Avramenko, L.A. Belyaeva, P.I. Semenyuk, M.A. Proskurnin, Improving the dispersity of detonation nanodiamond: differential scanning calorimetry as a new method of controlling the aggregation state of nanodiamond powders, Nanoscale 5 (4) (2013) 1529–1536.
[35] I. Larionova, V. Kuznetsov, A. Frolov, O. Shenderova, S. Moseenkov, I. Mazov, Properties of individual fractions of detonation nanodiamond, Diam. Relat. Mater. 15 (11) (2006) 1804–1808.
[36] W. Peng, R. Mahfouz, J. Pan, Y. Hou, P.M. Beaujuge, O.M. Bakr, Gram-scale fractionation of nanodiamonds by density gradient ultracentrifugation, Nanoscale 5 (11) (2013) 5017–5026.
[37] O. Shenderova, I. Petrov, J. Walsh, V. Grichko, V. Grishko, T. Tyler, G. Cunningham, Modification of detonation nanodiamonds by heat treatment in air, Diam. Relat. Mater. 15 (11) (2006) 1799–1803.
[38] N. Komatsu, Novel and practical separation processes for fullerenes, carbon nanotubes and nanodiamonds, J. Jpn. Pet. Inst. 52 (3) (2009) 73–80.
[39] S. Chukhaeva, Synthesis, properties, and applications of fractionated

nanodiamonds, Phys. Sol. State 46 (4) (2004) 625–628.
[40] I. Larionova, A. Frolov, L. Poleva, N. Bychin, Study of the composition and physicochemical properties of diamond hydrogels, Colloid J. 66 (3) (2004) 372–374.
[41] O.A. Williams, J. Hees, C. Dieker, W. Jäger, L. Kirste, C.E. Nebel, Size-dependent reactivity of diamond nanoparticles, ACS Nano 4 (8) (2010) 4824–4830.
[42] G. Mikheev, V. Vanyukov, T. Mogileva, The effect of the size factor of nanodiamonds in suspensions on optical power limiting and nonlinear laser light scattering, Technical Phys. Lett. 39 (3) (2013) 229–232.
[43] A.E. Aleksenskii, A.V. Shvidchenko, E.D. Eidel'man, The applicability of dynamic light scattering to determination of nanoparticle dimensions in sols, Technical Phys. Lett. 38 (12) (2012) 1049–1052.
[44] T.A. Filimonova, D.S. Volkov, M.A. Proskurnin, I.M. Pelivanov, Optoacoustic spectroscopy for real-time monitoring of strongly light-absorbing solutions in applications to analytical chemistry, Photoacoustics 1 (3–4) (2013) 54–61.
[45] I.M. Pelivanov, M.I. Barskaya, N.B. Podymova, T.D. Khokhlova, A.A. Karabutov, Opto-acoustic measurement of the local light absorption coefficient in turbid media: 2. On the possibility of light absorption coefficient measurement in a turbid medium from the amplitude of the opto-acoustic signal, Quant. Electron. 39 (9) (2009) 835.
[46] D.A. Nedosekin, M. Sarimollaoglu, E.I. Galanzha, R. Sawant, V.P. Torchilin, V.V. Verkhusha, J. Ma, M.H. Frank, A.S. Biris, V.P. Zharov, Synergy of photoacoustic and fluorescence flow cytometry of circulating cells with negative and positive contrasts, J. Biophoton. (2012) 425–434.
[47] D.A. Nedosekin, E.I. Galanzha, S. Ayyadevara, R.J. Shmookler Reis, V.P. Zharov, Photothermal confocal spectromicroscopy of multiple cellular chromophores and fluorophores, Biophys. J. 102 (3) (2012) 672–681.
[48] A.A. Oraevsky, A.A. Karabutov, A.A. Oraevsky (Ed.), Ultimate Sensitivity of Time-Resolved Optoacoustic Detection, SPIE, San Jose, CA, USA, 2000, pp. 228–239.
[49] M.V. Korobov, M.M. Batuk, N.V. Avramenko, N.I. Ivanova, N.N. Rozhkova, E. Ōsawa, Aggregate structure of "single-nano buckydiamond" in gel and dried powder by differential scanning calorimetry and nitrogen adsorption, Diam. Relat. Mater. 19 (5–6) (2010) 665–671.
[50] T.D. Khokhlova, I.M. Pelivanov, O.A. Sapozhnikov, V.S. Solomatin, A.A. Karabutov, Opto-acoustic diagnostics of the thermal action of high-intensity focused ultrasound on biological tissues: the possibility of its applications and model experiments, Quant. Electron. 36 (12) (2006) 1097.
[51] 17025:2005 General Requirements for the Competence of Testing and Calibration Laboratories, ISO/IEC, (2005).
[52] IUPAC - Stability Constant Database, Royal Society of Chemistry. SCQuery, Version 1.38, (1994).
[53] K. Ishikiriyama, M. Todoki, K. Motomura, Pore size distribution (PSD) measurements of silica gels by means of differential scanning calorimetry: I. Optimization for determination of PSD, J. Colloid Interface Sci. 171 (1) (1995) 92–102.
[54] CRC Handbook of Chemistry and Physics, 77th ed., CRC Press, Boca Raton, FL, 1996.
[55] M.V. Korobov, N.V. Avramenko, A.G. Bogachev, N.N. Rozhkova, E. Osawa, Nanophase of water in nano-diamond gel, J. Phys. Chem. C 111 (20) (2007) 7330–7334.
[56] V.Y. Osipov, M. Baidakova, K. Takai, T. Enoki, A. Vul, Magnetic properties of hydrogen-terminated surface layer of diamond nanoparticles, fullerenes, Nanotubes Carbon Nanostruct. 14 (2-3) (2006) 565–572.
[57] D.A. Nedosekin, E.I. Galanzha, S. Ayyadevara, R.J. Shmookler Reis, V.P. Zharov, Photothermal confocal spectromicroscopy of multiple cellular chromophores and fluorophores, Biophys. J. 102 (3) (2012) 672–681.
[58] E.I. Galanzha, V.P. Zharov, Photoacoustic flow cytometry, Methods 57 (3) (2012) 280–296.
[59] V.P. Zharov, Ultrasharp nonlinear photothermal and photoacoustic resonances and holes beyond the spectral limit, Nat. Photonics 5 (2) (2011) 110–116.
[60] V.V. Tuchin, A. Tárnok, V.P. Zharov, In vivo flow cytometry: A horizon of opportunities, Cytometry A 79A (10) (2011) 737–745.
[61] D. Razansky, A. Buehler, V. Ntziachristos, Volumetric real-time multispectral optoacoustic tomography of biomarkers, Nat. Protocols 6 (8) (2011) 1121–1129.
[62] D.M. Todorovic, M. Pawlak, I. Delgadillo-Holtfort, J. Pelzl, Photoacoustic and photothermal radiometry spectra of implanted Si wafers, Eur. Phys. J. Special Topics 153 (2008) 259–262.
[63] A.A. Karabutov, I.M. Pelivanov, N.B. Podymova, S.E. Skipetrov, Determination of the optical characteristics of turbid media by the laser optoacoustic method, Quant. Electron. 29 (12) (1999) 1054.
[64] P.S. Grashin, A.A. Karabutov, A.A. Oraevsky, I.M. Pelivanov, N.B. Podymova, E.V. Savateeva, V.S. Solomatin, Distribution of the laser radiation intensity in turbid media: Monte Carlo simulations, theoretical analysis, and results of optoacoustic measurements, Quant. Electron. 32 (10) (2002) 868.
[65] I.M. Pelivanov, S.A. Belov, V.S. Solomatin, T.D. Khokhlova, A.A. Karabutov, Direct opto-acoustic in vitro measurement of the spatial distribution of laser radiation in biological media, Quant. Electron. 36 (12) (2006) 1089.
[66] A.A. Karabutov, N.B. Podymova, V.S. Letokhov, Time-resolved laser optoacoustic tomography of inhomogeneous media, Appl. Phys. B 63 (6) (1996) 545–563.
[67] V.E. Gusev, A.A. Karabutov, Laser optoacoustics, Am. Inst. Phys. (1993).
[68] M. Qu, S. Mallidi, M. Mehrmohammadi, R. Truby, K. Homan, P. Joshi, Y.-S. Chen, K. Sokolov, S. Emelianov, Magneto-photo-acoustic imaging, Biomed. Opt. Express 2 (2) (2011) 385–396.
[69] S.Y. Emelianov, P.-C. Li, M. O'Donnell, Photoacoustics for molecular imaging and therapy, Phys. Today 62 (5) (2009) 34–39.
[70] C. Li, L.V. Wang, Photoacoustic tomography and sensing in biomedicine, Phys. Med. Biol. 54 (19) (2009) R59.
[71] L. Wang, Photoacoustic Imaging and Spectroscopy, Optical Science and Engineering, CRC Press, Boca Raton, 2009, p. 518.
[72] L.V. Wang, S. Hu, Photoacoustic tomography: in vivo imaging from organelles to organs, Science 335 (6075) (2012) 1458–1462.
[73] K.V. Lobko, M.A. Shishkin, T.A. Filimonova, D.S. Volkov, I.M. Pelivanov, M.A. Proskurnin, Optoacoustic determination of analytical parameters and physicochemical constants in highly concentrated solutions of chromophores, Talanta 174 (2017) 206–213.
[74] F.R. Lamastra, M.L. Grilli, G. Leahu, A. Belardini, R. Li Voti, C. Sibilia, D. Salvatori, I. Cacciotti, F. Nanni, Photoacoustic spectroscopy investigation of zinc oxide/diatom frustules hybrid powders, Int. J. Thermophys. 39 (9) (2018) 110.
[75] F.R. Lamastra, M.L. Grilli, G. Leahu, A. Belardini, R. Li Voti, C. Sibilia, D. Salvatori, I. Cacciotti, F. Nanni, Diatom frustules decorated with zinc oxide nanoparticles for enhanced optical properties, Nanotechnology 28 (37) (2017) 375704.
[76] S.V. Koniakhin, N.A. Besedina, D.A. Kirilenko, A.V. Shvidchenko, E.D. Eidelman, Ultracentrifugation for ultrafine nanodiamond fractionation, Superlattices Microstruct. 113 (2018) 204–212.

Liliya Usoltseva is a post-graduate student at the Chemistry department of M.V. Lomonosov Moscow State University. Her work relates to the development of methodological aspects of photothermal and optoacoustic techniques in physical chemistry and chemical analysis of nanodiamonds, fullerenes, and other nanomaterials.

Dmitry Volkov, Ph.D., is a Research Scientist at the Chemistry department of M.V. Lomonosov Moscow State University. He published more than 60 scientific papers in peer-reviewed journals. His fields of scientific interests: molecular and atomic spectroscopy, disperse systems, humic substances, nanomaterials, physicochemical studies of carbon nanomaterials, photothermal spectroscopy.

Dmitry Nedosekin, Ph.D., is a Research Associate at the Phillips Classic Laser & Nanomedicine Laboratories, University of Arkansas for Medical Sciences. He completed doctoral training at the Philipps-Universität Marburg, Germany (2004–2005) and at the M.V. Lomonosov Moscow State University, Russia (2003–2007) and received a Ph.D. degree on Analytical Chemistry. His scientific interests cover a wide range of biophotonic methods including the development of instrumentation that integrates fluorescence, photothermal, photoacoustic, and Raman spectroscopy techniques for biomedical imaging and in-flow analysis.

Mikhail Korobov, Ph.D., D.Sc., is a Professor at the Chemistry department of M.V. Lomonosov Moscow State University. He received his Ph.D. and D.Sc. degrees from this university. He is the author of 2 books and 200+ papers on nanomaterials and chemical thermodynamics. He is the main lecturer of the Course of physical chemistry (thermodynamics and kinetics) for 3-rd and 4-th year students of the Chemistry Department of M.V. Lomonosov Moscow State University. His scientific interests are in the theoretical basis of disperse systems of nanodiamonds, nanotubes, and fullerenes, the thermodynamical calculations in these systems, physical chemistry of nanodiamond surface, nanofluids.

Mikhail Proskurnin, Ph.D, DSc, is a Professor at the Chemistry department of M.V. Lomonosov Moscow State University. He received his Ph.D. and D.Sc. degrees from this university, and was a Visiting Scientist in Tokyo University (1999–2000), FZK (Germany, 2002), and UAMS (AK, USA, 2012). He is a Professor of the Russian Academy of Sciences and a member of The Bureau of The Scientific Council on Analytical Chemistry of The Russian Academy of Sciences. He is the author and translator of 11 books, 5 patents and 180+ papers on photothermal spectroscopy and analytical chemistry. The scientific interests of Prof. Proskurnin lie in the photonics, and the development of photothermal spectroscopy in analytical and physical chemistry and applied materials science and biomedical studies.

Vladimir P. Zharov, Ph.D, DSc, is the director of the Arkansas Nanomedicine Center, a Professor of Biomedical Engineering (BME) and Josephine T. McGill Chair in Cancer Research at the University of Arkansas for Medical Sciences (UAMS), the USA. He received his pH.D.and D.Sc. degrees from Bauman Moscow State Technical University (BMSTU), completed a postdoctoral fellowship at Lawrence Berkeley National Laboratory of the University of California and served as the Chairman of the BME department at BMSTU. He is the author of 5 books, 52 patents, and more than 200 papers in the field of laser spectroscopy, biophotonics, and nanomedicine including six publications in the Nature family journals. He is one of the pioneers of high resolution photoacoustic spectroscopy and the inventor of photoacoustic tweezers, pulse nanophotothermolysis of infections and cancer, and in vivo multicolor flow cytometry. Dr. Zharov is the principle investigator on 16 NIH (5R01), NSF, and other agency grants. His laser-based technologies have been commercialized and used in clinics. Dr. Zharov is the State Prize Winner in Russia, the most prestigious national award in Russia, and the first recipient of the U.S. Maiman Award named after the inventor of the first laser.